Plasma degradation of water organic pollutants: Ab-initio molecular dynamics simulations and experiments

Pascal Brault, Florin Bilea, Monica Magureanu, Corina Bradu, Olivier Aubry, Hervé Rabat, Dunpin Hong

Received: 3 July 2023 | Revised: 28 July 2023 | Accepted: 28 July 2023

DOI: 10.1002/ppap.202300116

RESEARCH ARTICLE

PLASMA PROCESSES AND POLYMERS

Plasma degradation of water organic pollutants: Ab initio molecular dynamics simulations and experiments

Pascal Brault[1] | **Florin Bilea**[2] | **Monica Magureanu**[2] | **Corina Bradu**[3] | **Olivier Aubry**[1] | **Hervé Rabat**[1] | **Dunpin Hong**[1]

[1]GREMI, CNRS—Université d'Orléans, Orléans, France

[2]Department of Plasma Physics and, Nuclear Fusion, National Institute for Lasers, Plasma and Radiation Physics, Bucharest, Romania

[3]Department of Systems Ecology and Sustainability, Faculty of Biology, University of Bucharest, Bucharest, Romania

Correspondence
Pascal Brault, GREMI, CNRS—Université d'Orléans, 14 rue d'Issoudun, Orléans, 45067 France.
Email: pascal.brault@univ-orleans.fr

Funding information
Romanian Ministry of Education and Research; Région Centre - Val de Loire, France; Conseil Régional Centre-Val de Loire, Grant/Award Number: #2021-00144786; CNCS-UEFISCDI, Grant/Award Number: PN-III-P4-ID-PCE-2020-0335

Abstract

Ab initio molecular dynamics simulations and experiments were carried out to study the interaction between plasma-produced hydroxyl radicals and organic pollutant molecules in wastewater. The simulation method was validated on the degradation products of phenol and further applied to the more complex molecule of sulfamethoxazole (SMX). The comparison with experimentally detected intermediate products obtained during plasma treatment of SMX solutions confirms the hydroxylation of the benzene and isoxazole rings observed in some of the simulations.

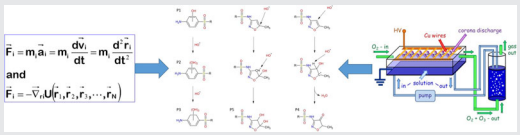

KEYWORDS

ab initio molecular dynamics, antibiotics, cold atmospheric plasma, phenol, plasma oxidation, reactive molecular dynamics, SMX, sulfamethoxazole, tandem mass spectrometry, wastewater treatment

1 | INTRODUCTION

Elimination of pollutants in water is a challenge worldwide, and efforts are being made to tackle this challenge with the use of nonthermal plasmas at atmospheric pressure. Various plasma sources efficiently produce reactive oxygen and nitrogen species (RONS) that interact with and subsequently degrade organic molecules. Since such phenomena are molecular in nature, reactive classical and ab initio molecular dynamics (AIMD) are relevant tools for analyzing the degradative oxidation processes involved.[1] The main actor among the plasma-generated RONS is the HO• radical, which efficiently and unselectively reacts with any organic molecule. The production of HO• in plasmas in contact with water is generally attributed to the electron impact dissociation of water molecules. However, other formation mechanisms are also possible, and some of them,

such as dissociative recombination reactions, can contribute considerably to HO• generation depending on the specific plasma properties.[2] Regardless of the plasma source used for water treatment, HO• is acknowledged to play the main role in the degradation.[3–5] Actually, all advanced oxidation processes (AOPs) rely on the formation of HO•.[6,7] The simulations performed in this study are carried out to describe and predict degradation products after interactions, in water, of selected molecules with the HO• radical, which is of crucial importance, since the products can also be harmful. Molecular dynamics (MD) simulations are generating considerable interest for the study of physical–chemical processes in plasmas.[8,9] This interest is motivated by the ability of these simulations to address the reactivity of relatively large molecular systems (up to 109 atoms). Since plasmas are able to produce radicals that interact with other species both in the gas phase and with solid and liquid surfaces, including in-diffusion, MD simulations are relevant for tracking such reactive processes. Unfortunately, it is not yet possible to directly include the electrons in MD. Despite this limitation, neutral–neutral, ion–neutral, and ion–ion interactions can be included with proper initial conditions, such as positions and velocities, required to solve the MD Newton equations of motion. Moreover, these initial conditions can be defined using plasma composition from experimental measurements, such as mass spectrometry, or from a fluid model.[10–13] Solving these equations only requires the knowledge of the interaction potentials and then the forces between each interacting species. There are two popular reactive force field families that describe chemical reactions, reaxFF and COMB3,[14] which address bond breaking and formation via a distance-dependent bond order. Moreover, these force fields implement a variable charge scheme that allows to address charge transfer. The main limitation is that these force fields are parametrized for a small set of molecules and they are not always transferable to any similar molecules or to other molecules containing the same atoms. When there is a lack of force fields due to the complexity of the involved molecules, coupling quantum-calculated force field calculations with MD simulations is the solution.[15] This is called ab initio or first-principles molecular dynamics (AIMD or FPMD). Basically, the force fields are calculated at every defined timestep using a quantum chemistry code (such as density functional theory [DFT], e.g., but not limited to it), after which an MD step is achieved. The main difficulty lies in choosing the most appropriate quantum chemistry method and basis sets. The main limitation is the computing time, which becomes very long when high accuracy is expected. The present work will thus address the interaction of the HO• radical with some selected molecules present in water using AIMD. To implement this method, we use the DFT in the tight-binding approach (DFTB), which is a computationally efficient DFT scheme for the ab initio step of calculating the forces between atoms. Moreover, we use the GFN1-xTB parametrization, which is optimized for geometries, frequencies, and noncovalent interactions and covers all elements of the periodic table up to radon.[16] To take into account the conditions of nonthermal plasma experiments as closely as possible, MD simulations are carried out at 300K with the periodic release of the HO• radical into water containing the selected pollutant molecule. Phenol (C_6H_5OH) and sulfamethoxazole (SMX) ($C_{10}H_{11}N_3O_3S$) oxidation processes by HO• in water are, investigated. Phenol is studied as a test molecule to formulate and validate the AIMD approach since there are significant data in the literature. An additional motivation for the selection of phenol is the toxicity of numerous phenolic compounds.[17,18] SMX is a widely used antibacterial antibiotic both in human healthcare and in animal breeding. It is present in water especially close to intensive farming areas[19–21] but also in hospital wastewater[22,23] and in the effluent from pharmaceutical plants.[24] Wastewater treatment plants fail to effectively remove SMX, as has been proven by its presence in the treated effluents,[23] and thus it is frequently found in surface waters,[23,25,26] groundwater, and tap water[23,27] and could pose an ecotoxicological risk to aquatic organisms[22] and contribute to the spread of antibiotic resistance.[26] For these molecules, the MD-simulated degradation products are compared with the available experimental ones detected using liquid chromatography–tandem mass spectrometry (LC–MS/MS). In summary, here, an AIMD simulation protocol is tested on a widely studied molecule, phenol, and applied on a more complex molecule, here SMX. Comparisons with the literature and the experiments reported here are presented.

2 | MOLECULAR DYNAMICS SIMUMATIONS

The initial simulation box size is $10 \times 10 \times 10$ Å^3, comprising one phenol or one SMX molecule with 15 H_2O molecules. This small number of water molecules is expected to be enough to represent the environment of the SMX molecules.[1] Ten HO• radicals are released one after another at random positions at a 2.5 Å minimum distance from the molecules already in the box. The integration time dt = 0.25 fs and the simulation lasts for 5×10^4 timesteps, that is, 12.5 ps. HO• are released every

4000 timesteps after an initial delay of 4000 timesteps. The simulations are carried out in the NPT ensemble (i.e., total atom number N, total pressure P, and temperature T are kept constant). This allows the maintenance of a constant water density when releasing HO• radicals. A Nose–Hoover thermostat is used to maintain the temperature at 300K. The damping time is 100 fs. A Martyna–Tobias–Klein barostat with a damping time of 500 fs is used to maintain the pressure at 10^5 Pa. Simulations are repeated 10 times after changing the initial positions and velocities of all molecules at the minimal starting time for statistical purposes. AIMD simulations have been carried out using the AMS suite from SCM company.[28]

3 | EXPERIMENTS

The experiments on SMX degradation were performed using a pulsed corona discharge above water with gas recycling. The system, described in detail in previous articles,[29,30] consists of two reactors connected in series, that is, the plasma reactor and the solution tank, through which the effluent gas from the discharge is bubbled. This method ensures enhanced contact between the oxidizing species produced in the plasma and the pollutant molecules, and thus remarkably improves degradation efficiency.[29] Plasma-generated ozone plays a major role in this setup. It can react directly with the organic contaminant, especially in the solution reservoir, where the bubbling considerably enhances the contact surface area as compared with the plasma reactor. More importantly, the peroxone process, that is, the reaction between ozone and hydrogen peroxide produced in plasma, generates additional HO• radicals outside of the plasma region. Previous results showed the formation of H_2O_2 in plasma-treated water but evidenced its absence in the case of gas recycling, as well as the elimination of externally added H_2O_2.[31,32] It was also observed that the concentration of HO radicals doubles in this setup as compared with plasma alone.[32] The corona discharge was generated in oxygen (flow rate of 300 mL/min), in a multi-wire-to-plate configuration, using an array of 20 copper wires (diameter of 100 μμμm) as a high-voltage electrode placed above the liquid surface, which was grounded. Based on a previous optimization study,[33] high-voltage pulses of 110 ns (full width at half maximum) and 18 kV amplitude were selected for these experiments. The pulse frequency was set to 25 Hz, and under these conditions, the power dissipated in the plasma was approximately 5 W. The SMX solution was prepared at a concentration of 0.5 mM in distilled water. The conductivity was adjusted to 300 μS/cm using $NaHCO_3$. A solution volume of 330 mL was treated for 60 min and samples were collected periodically (2, 5, 10, 20, 40, and 60 min) during the treatment. The pollutant concentration was measured by high-performance liquid chromatography (HPLC) using a Rigol L-3000 system equipped with an RP-C18 column (250 × 4.6 mm, 5 μm) maintained at 27°C. The mobile phase consisted of 30% acetonitrile and 70% water (with 0.1% formic acid). The measurements were done at 270 nm using a diode array detector. The degradation products of SMX were studied using an Agilent 1260 Infinity II HPLC coupled with a 6530 QTOF detector. The separation was achieved using an Eclipse C18 Plus column (150 × 3 mm, 3.5 μm) maintained at 25°C. The mobile phase consisted of acetonitrile and water (with 0.1% formic acid) and was varied over the course of 25 min from 5% to 20% acetonitrile while maintaining a constant flow of 0.4 mL/min. The parameters of the electrospray ionization (ESI) source were set as follows: capillary voltage at 3500 V, nozzle voltage at 1000 V, gas temperature at 300°C, gas flow at 8 L/min, sheath gas temperature at 350°C, sheath gas flow at 11 L/min, and nebulizer at 35 psig. MS and MS/MS spectra were recorded in the range 50–1000 (mass/charge), for both positive and negative ions, at a rate of three spectra/second and one spectrum/second, respectively. The collision energy was varied between 0 and 20 eV.

4 | RESULTS

4.1 | Phenol

Phenol (C_6H_5OH) is one of the simplest cyclic molecules. Its oxidation degradation routes have been studied experimentally and there is a consensus on oxidation steps and products.[34] These experimentally determined steps and products are summarized in Figure 1.

Phenol degradation has been studied in numerous plasma systems utilizing electrical discharges generated directly in water or in gas–liquid environments. A summary of this research with respect to the intermediate products and reaction mechanism is provided in Locke et al.[35]. The majority of the studies report that the plasma oxidation of phenol in water occurs through a reaction with hydroxyl radicals, which electrophillically attack the phenol molecule. The authors suggest the formation of a transient dihydroxycyclohexadienyl radical as a result of this attack, which may further react, finally leading to hydroxylated products of phenol, such as catechol, hydroquinone, and benzoquinone. Further oxidation of these intermediates to trihydroxybenzenes, such as pyrogallol, hydroxyhydroquinone, and phloroglucinol, represents the next step in the

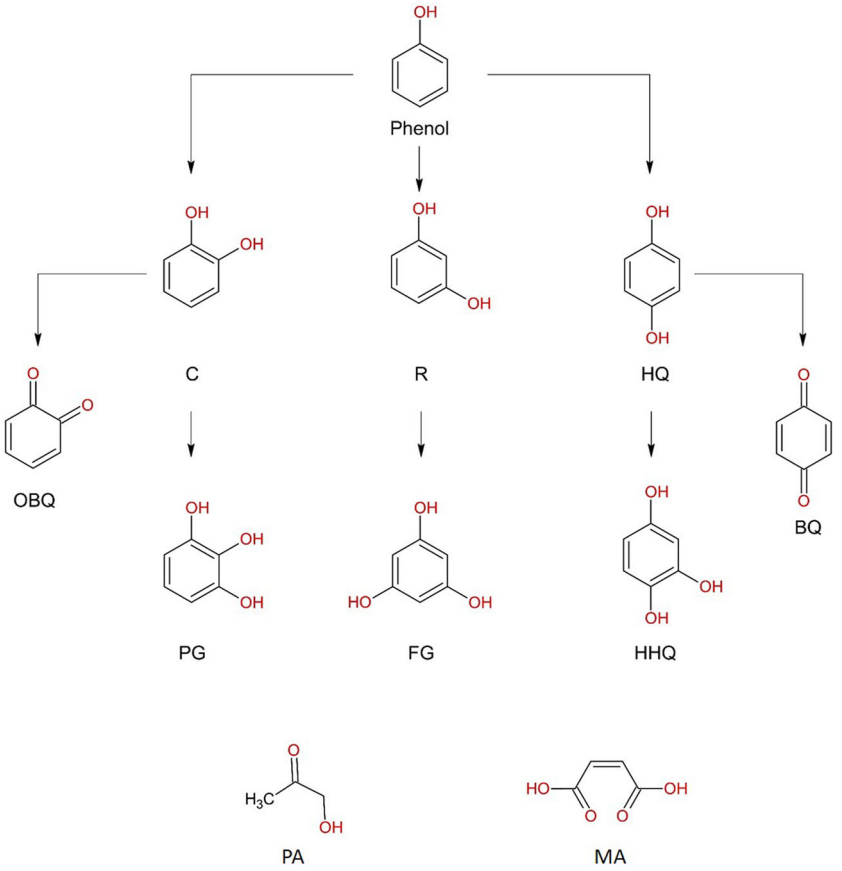

FIGURE 1 Summary of the reported phenol oxidation steps and corresponding products: catechol (C), resorcinol (R), hydroquinone (HQ), 1,4-benzoquinone (BQ), 1,2-benzoquinone (OBQ), pyrogallol (PG), phloroglucinol (FG), hydroxyhydroquinone (HHQ), pyruvic acid (PA), and maleic acid (MA). Adapted from Villasenor.[34]

reaction pathway. Various ring-cleavage products were also typically reported in phenol solutions exposed to plasma, the most frequent being organic acids such as maleic, oxalic, and formic acids.

AIMD simulations consist of 10 runs with different random initial conditions for positions and velocities. The latter are randomly selected in a Maxwell–Boltzmann distribution at a temperature of 300 K. The first oxidation step by HO• leads to four catechol (C) molecules, four resorcinol (R) molecules, one hydroquinone (HQ) molecule, and one phenyl hydroperoxide molecule, on analyzing the 10-run results (Figure 2). When looking at the next steps, three hydroxyhydroquinone (HHQ) molecules and two pyrogallol (PG) molecules are created in 5 of the 10 runs (not shown in Figure 2). In the other five remaining runs, four molecules are created as shown in Figure 2. These molecules are evolving toward cycle breaking after additional HO• release, while HHQ and PG are instead further hydroxylated. When comparing Figures 1 and 2, it is clear that this phenol oxidation study, using AIMD, is thus able to reproduce the main phenol oxidation products. Therefore, the present simulation protocol can be applied to more complex organic pollutants, such as SMX in this study.

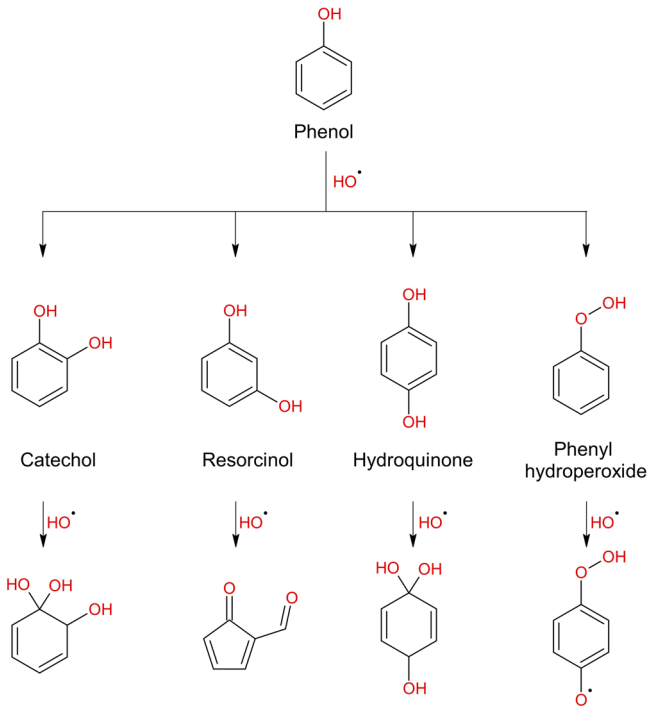

FIGURE 2 Molecular dynamics (MD) simulations obtained products after interaction with HO•.

4.2 | Sulfamethoxazole

4.2.1 | Experiments

Figure 3 shows the degradation of SMX in water, more precisely, the variation of the relative concentration and the logarithmic representation (inset) as a function of plasma treatment time. The decrease in the concentration is well described by a first-order decay exponential function. The first-order kinetics is confirmed by the logarithmic representation, with an apparent reaction rate constant $k_{obs} = 0.205\,min^{-1}$. Almost complete removal of the initial 0.5 mM SMX was achieved after 20 min of exposure to plasma, while the half-life time (i.e., the time needed to degrade half of the initial concentration of contaminant) was approximately 5 min. A useful parameter for evaluation of the treatment efficiency is the energy yield, defined as the amount of contaminant removed per unit of energy spent in the process and usually measured either at 50% or, more frequently, at 90% removal of the target compound. In our case, a value of 32 g/kWh was obtained at 90% SMX removal.

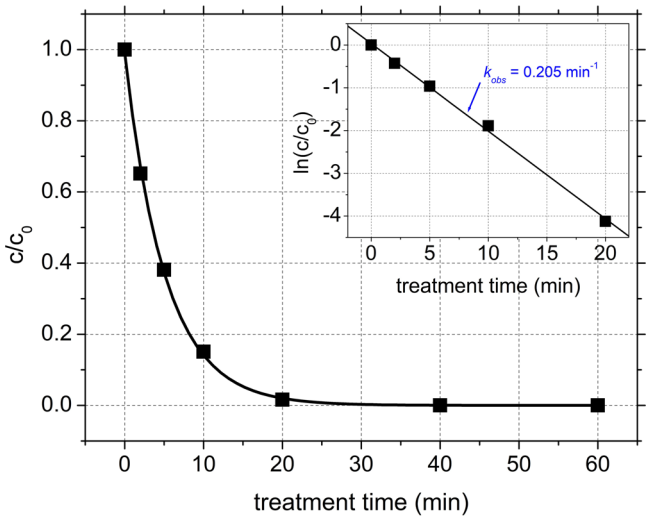

FIGURE 3 The decrease of the sulfamethoxazole (SMX) concentration as a function of time. Inset: logarithmic representation of the degradation as a function of treatment time.

Identification of SMX degradation products was done based on the MS/MS fragmentation patterns recorded. Several hydroxylated compounds have been observed and these are shown in Figure 4. The only compounds detected in the solution as a result of treatment are the ones on the first row, referred to as P1–P5. The masses of the products, as seen in the solution, are P1-269 amu, P2-285 amu, P3-301 amu, P4-269 amu, and P5-287 amu, all of them detected either as positive ions (+1 amu) or as negative ions (−1 amu). The second and third rows in Figure 4 show fragments of these compounds obtained during the analysis as a result of the fragmentation in the ESI source. When considering the HO• reaction with SMX, the two cycles in the compound's structure (the benzene and isoxazole rings) appear to act independently of each other. As such, the degradation products can be grouped based on the attack site of HO• into two degradation paths: hydroxylation of benzene (P1–P3) and hydroxylation of the isoxazole ring (P4–P5). The first path starts with the formation of compound P1 (2 isomers) with a mass spectrum containing the *m/z*+ values 172, 124, and 108. These fragments are consistent with the presence of a hydroxyl group on the benzene ring as shown in Figure 4. Using the same reasoning, the di-hydroxylated P2 and tri-hydroxylated P3 have been

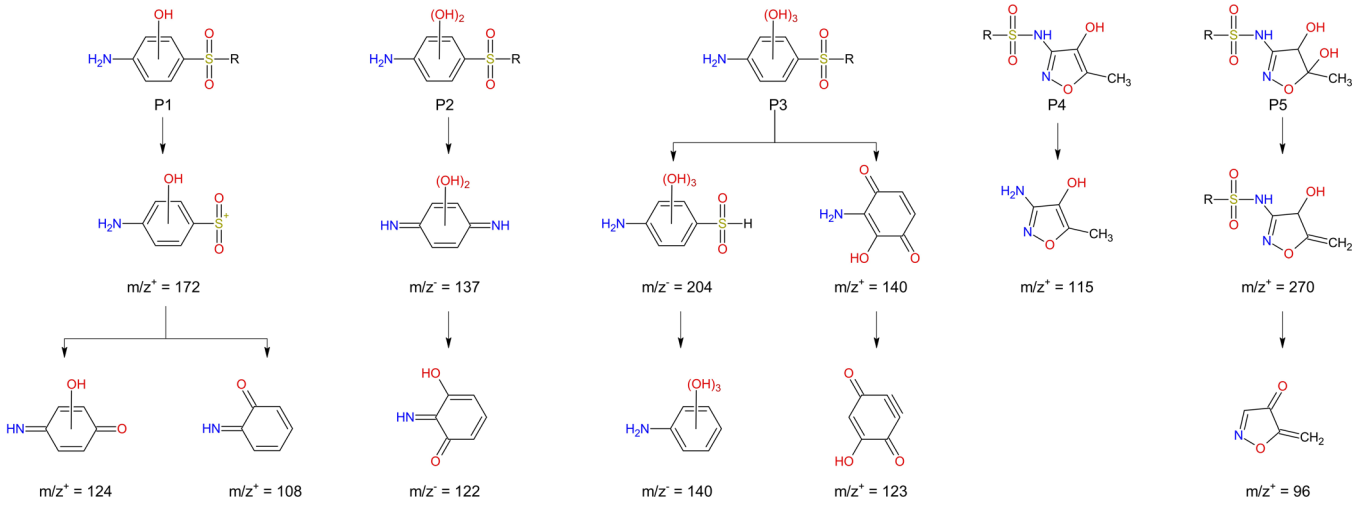

FIGURE 4 MS/MS fragmentation patterns of the hydroxylated degradation products of sulfamethoxazole obtained during plasma treatment.

identified. The mass spectrum of P2 contains fragments with *m/z*- values of 137 and 122, while the one attributed to P3 includes *m/z*- 204 and 140 and *m/z*+ 140 and 123. Thus, the HO• attack on the benzene ring describes a sequential hydroxylation of SMX. The attachment of HO• onto the isoxazole ring initiates the second degradation path. In this case, the formation of the mono-hydroxylated P4 degradation product was confirmed due to the presence of the 115 *m/z*+ fragment in the compound's mass spectrum. The addition of a HO• radical to P4 results in the formation of P5. During its fragmentation, the compound loses a water molecule and forms the *m/z*+ 270 ion, which undergoes C–N bond cleavage, resulting in a *m/z*+ 96 ion.

4.2.2 | Ab initio Molecular Dynamics

The SMX oxidation process in water is determined using the previous AIMD procedure for phenol, that is, 10 runs with different initial conditions, as for phenol in the previous section. The HO• radical is injected every 1 ps and 10 times. A total of 1 ps relaxation is ran before the first HO• injection and 2.5 ps is lasting after the tenth released HO•. Table 1 shows the recorded masses of compounds issued from SMX, which can be further compared with mass spectrometry measurements. Bold numbers correspond to masses recorded in the present experiments and underlined ones have a potential match. Figure 5 shows chemical structures corresponding to the main AIMD-simulated hydroxylated products. The resulting simulated product mass ranges 265–270, 282–286, and 298–303 (all runs) correspond to hydroxylation with 1, 2, and 3 HO•, respectively, either on the benzene ring or on the isoxazole ring, as in experiments. AIMD simulations predict mass in the range of 315–319 and 335–336, corresponding to 4 and 5 additional attached HO• radicals to SMX. Such mass ranges, 3–5 atomic mass units wide, arise due to transient conditions with unrelaxed compounds. For comparison, with mass spectrometry measurements, results can differ in some unit values, without being false. From Table 1, it can be seen that larger masses result in the fragmentation of these multiple hydroxylated SMX. S–C bond breakage occurs after a HO• radical makes contact with a S, SO, or C atom adjacent to S atom, resulting in dissociation into fragments with masses ranging from 108 to 196. Fragmentation occurs (masses less than 253 amu) during 4 runs over the 10 runs performed. In one occurrence, three fragments are obtained (run #7).

TABLE 1 List of the masses (amu) after HO• release.

	m_0 0–1ps	m_1 1–2ps	m_2 2–3ps	m_3 3–4ps	m_4 4–5ps	m_5 5–6ps	m_6 6–7ps	m_7 7–8ps	m_8 8–9ps	m_9 9–10ps	m_{10} 10–12.5ps
Run #1	253	252	269	268	267	267	266	265	282	299	315
Run #2	253	**269**	**269**	268	**285**	284	301	299	299	298	315
Run #3	253	252	269	286	285	302	301	318	301	300	285
											32
Run #4	253	253	**269**	268	268	251	251	251	285	333	333
Run #5	253	252	**269**	**269**	108	108	126	126	125	123	140
					176	176	192	192	192	192	192
Run #6	253	253	**269**	268	285	302	319	336	157	156	70
									195	195	103
											196
Run #7	253	253	**270**	286	302	302	303	320	319	318	317
Run #8	253	**270**	269	268	267	284	63	63	317	81	82
							237	236		253	269
Run #9	253	252	**269**	286	303	320	337	336	157	174	173
									196	196	196
Run #10	253	253	269	269	269	269	269	269	269	285	317

Note: m_i is/are the mass(es) obtained after the injection of the i^{th} HO• in the corresponding time interval (in the form t_i-t_i + 1 ps). Bold masses are confirmed by experiments. Underlined masses have a potential match.

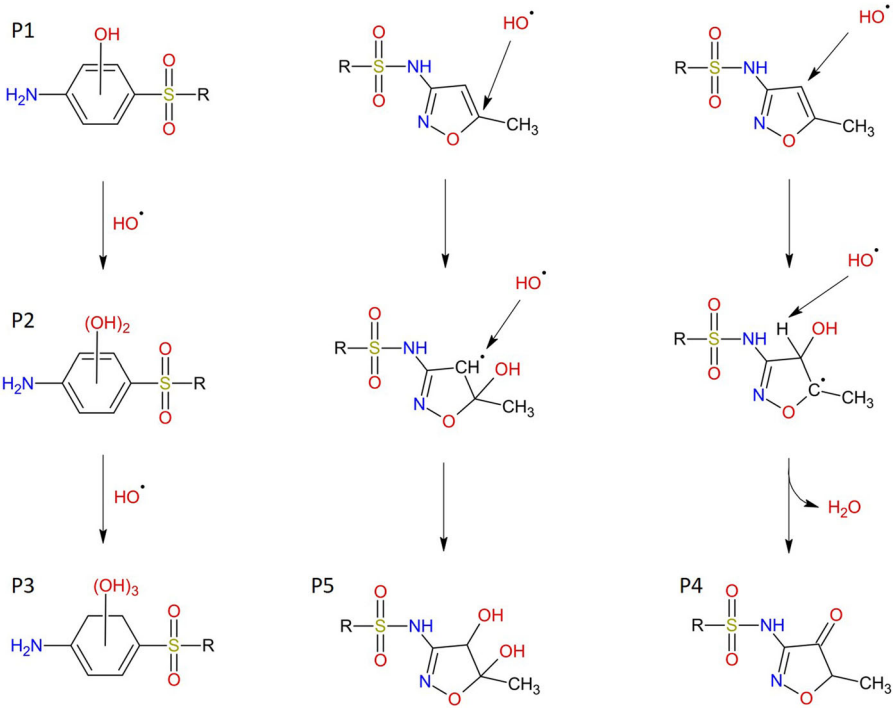

FIGURE 5 The main hydroxylation reactions observed during the simulations of sulfamethoxazole oxidation leading to observed products P1–P5 of Figure 4.

5 | DISCUSSION

The main recorded high masses (> 253 amu) have already been reported in experiments such as the ultrasound/ozone oxidation process,[19] photocatalytic,[36] nonthermal plasmas,[4,37–45] and a combination of AOPs.[46] Most of the AIMD simulations and the present experimental results show changes of either or both cycles, while the S–N bond is rarely affected. As such, the two cycles can be treated as separate entities that can react with hydroxyl radicals alternatively or simultaneously, leading to the formation of several mono-, di-, tri-, tetra-, and penta-hydroxylated compounds over the course of the AIMD simulations. Hydroxylation of the benzene ring (Figure 5) occurs as one of the first steps during degradation. This leads to the formation of several isomers depending on the attack site of the hydroxyl radicals. As a result of plasma-driven SMX degradation, at least two of these isomers are formed, with a mass of 269 amu. Formation of these isomers was observed in simulation runs #4 and #9. The attack of hydroxyl radicals on the isoxazole ring occurs alternatively on either side of the C=C bond, forming the mono-hydroxylated P4 (run #6 and #8) and the di-hydroxylated P5 (run #7 and #9). Benzene hydroxylation occurs simultaneously with the hydroxyl attack on the isoxazole cycle during simulation runs #2, #3, #6, #7, #8, and #9. A comparison of Figures 4 and 5 thus shows a reasonable agreement between AIMD and (MS/MS) experiments regarding hydroxylation steps. However, the fragmentation of the pollutant molecule observed in AIMD, with fragment masses 63, 70, 81–82, 108, 124, 140, 157, and 172–174, could not be correlated with the experimental results. Nevertheless, fragment masses 108, 156, and 172 have been previously detected (figs. 12 and 13 from Kim et al.[20]). It is possible that fragments formed during plasma degradation of SMX are not detected with the chromatographic method used. It should also be mentioned that, while AIMD accounts for the contribution of hydroxyl radicals toward pollutant removal, plasma also generates a series of other reactive species (ozone, hydrogen peroxide, hydroperoxyl radical, etc.) that could be involved in the degradation of SMX, generating different degradation products other than HO•.[47] Thus, a perfect correlation cannot be expected. Another explanation for the observed discrepancies could stem from the timeline of the reactions. During the plasma experiments, the abundance of the pollutant molecules, chemical species (oxygen, ions, etc.), and the higher volume allow the formation of stable products between successive hydroxyl radical attacks. Translation of this process into AIMD is not simple and requires a compromise due to the computational power needed to take these parameters into account. As such, some of the degradation products (Table 1) are organic radicals and peroxides, which could represent the unstable intermediaries of chemical reactions that cannot be experimentally detected. Thus, the main advantage of the AIMD method is that its use can provide insight into

the chemical reactions and its complementarity toward the experimental results.

6 | CONCLUSIONS

AIMD simulations are conducted for providing prediction of degradation products in water by HO• radicals. These include the periodical release of HO• radicals in a simulation box containing one organic pollutant molecule (here phenol or SMX was used in this study) surrounded by enough water molecules to mimic the pollutant molecule in an aqueous environment. This method has been validated by reproducing the first step of phenol hydroxylation. The second step of hydroxylation provides additional products compared to that reported in the literature. Use of the methodology, defined for phenol, for an SMX antibiotic molecule, leads to hydroxylation steps with 1, 2, and 3 HO• radicals, well-reproducing plasma ozonation experiments as well as experiments reported in the literature. With SMX fragmentation, the plasma experiments fail to correlate to the AIMD results. Nevertheless, expanding the comparison to include fragments reported in the literature indicates additional agreements between AIMD simulations and experiments. The differences between experiments and simulations could have arisen as a result of too short simulation times, preventing the relaxation of intermediate compounds. They can also stem from the fact that AIMD simulations only consider HO• radical interactions with pollutant molecules, and thus do not account for other reactive species simultaneously produced in the experiments. Thus, the methodology can be successfully applied to predict the initial attacks of hydroxyl radicals on the organic pollutant molecule and to gain insight into the mechanistic aspects of the reactions. These results are promising, considering that the initial change in the chemical structure of a target compound is what most studies consider as pollutant removal. This method can be used for all AOPs, which are based on hydroxyl radical reactions. The same procedure can be easily extended to other active species produced by cold atmospheric plasmas (O_3, O•, NO_x, etc.), both neutral and ions.

AUTHOR CONTRIBUTIONS

Pascal Brault developed and ran simulations and wrote simulation parts and the draft of the manuscript. Florin Bilea conducted the experiments and wrote experimental parts of the manuscript. Monica Magureanu and Corina Bradu supervised the experiments and contributed to the writing of the manuscript. Olivier Aubry, Dunpin Hong, and Hervé Rabat contributed to the writing of the manuscript.

ACKNOWLEDGMENTS

Part of this work was supported by Conseil Régional Centre-Val de Loire with grant #2021-00144786 for project Perturb'Eau. The experimental work was supported by a grant from the Romanian Ministry of Education and Research, CNCS - UEFISCDI, project number PN-III-P4-ID-PCE-2020-0335, within PNCDI III.

CONFLICT OF INTEREST STATEMENT

The authors declare no conflict of interest.

DATA AVAILABILITY STATEMENT

The data that support the findings of this study are available from the corresponding author upon reasonable request.

ORCID

Pascal Brault http://orcid.org/0000-0002-8380-480X

REFERENCES

[1] P. Brault, M. Abraham, A. Bensebaa, O. Aubry, D. Hong, H. Rabat, M. Magureanu, *J. Appl. Phys.* **2021**, *129*(18), 183304.
[2] P. Bruggeman, D. C. Schram, *Plasma Sources Sci. Technol.* **2010**, *19*(4), 045025.
[3] P. Vanraes, A. Bogaerts, *Appl. Phys. Rev.* **2018**, *5*(3), 031103.
[4] M. Magureanu, F. Bilea, C. Bradu, D. Hong, *J. Hazard. Mater.* **2021**, *417*, 125481.
[5] N. Morin-Crini, E. Lichtfouse, M. Fourmentin, A. R. L. Ribeiro, C. Noutsopoulos, F. Mapelli, É. Fenyvesi, M. G. A. Vieira, L. A. Picos-Corrales, J. C. Moreno-Piraján, L. Giraldo, T. Sohajda, M. M. Huq, J. Soltan, G. Torri, M. Magureanu, C. Bradu, G. Crini, *Environ. Chem. Lett.* **2022**, *20*(2), 1333.
[6] M. Klavarioti, D. Mantzavinos, D. Kassinos, *Environ. Int.* **2009**, *35*(2), 402.
[7] M. A. Oturan, J. -J. Aaron, *Crit. Rev. Environ. Sci. Technol.* **2014**, *44*(23), 2577.
[8] E. Neyts, P. Brault, *Plasma Process. Polym.* **2017**, *14*, 1–2, 1600145.
[9] M. Bonitz, A. Filinov, J. W. Abraham, K. Balzer, H. Kählert, E. Pehlke, F. X. Bronold, M. Pamperin, M. Becker, D. Loffhagen, H. Fehske, Front. Chem. Sci. Eng. **2019**, *13*(2), 201.
[10] M. Zarshenas, K. Moshkunov, B. Czerwinski, T. Leyssens, A. Delcorte, *J. Phys. Chem. C* **2018**, *122*(27), 15252.
[11] P. Brault, M. Ji, D. Sciacqua, F. Poncin-Epaillard, J. Berndt, E. Kovacevic, *Plasma Process. Polym.* **2022**, *19*(1), 2100103.
[12] G. Tetard, A. Michau, S. Prasanna, J. Mougenot, P. Brault, K. Hassouni, *Plasma Sources Sci. Technol.* **2021**, *30*(10), 105015.
[13] G. Tetard, A. Michau, S. Prasanna, J. Mougenot, P. Brault, K. Hassouni, *Plasma Process. Polym.* **2022**, *19*(5), 2100204.

[14] T. Liang, Y. K. Shin, Y. T. Cheng, D. E. Yilmaz, K. G. Vishnu, O. Verners, C. Zou, S. R. Phillpot, S. B. Sinnott, A. C. Van Duin, *Annu. Rev. Mater. Res.* **2013**, *43*1, 109.
[15] D. Marx, J. Hutter, in *Ab Initio Molecular Dynamics: Theory and Implementation, in Modern Methods and Algorithms of Quantum Chemistry* (Ed: J Grotendorst), Publication Series of the John von Neumann Institute for Computing, Forschungzentrum Juelich, Vol. 22, **2004**.
[16] S. Grimme, C. Bannwarth, P. Shushkov, *J. Chem. Theory Comput*. **2017**, *13*(5), 1989.
[17] N. Panigrahy, A. Priyadarshini, M. M. Sahoo, A. K. Verma, A. Daverey, N. K. Sahoo, *Environ. Technol. Innov*. **2022**, *27*, 102423.
[18] R. M. Bruce, J. Santodonato, M. W. Neal, *Toxicol. Ind. Health* **1987**, *3*(4), 535.
[19] W. Q. Guo, R. L. Yin, X. J. Zhou, J. S. Du, H. O. Cao, S. S. Yang, N. Q. Ren, *Ultrason. Sonochem*. **2015**, *22*, 182.
[20] K. S. Kim, S. K. Kam, Y. S. Mok, *Chem. Eng. J*. **2015**, *271*, 31.
[21] G. Prasannamedha, P. S. Kumar, *J. Clean. Prod*. **2020**, *250*, 119553.
[22] L. H. Santos, M. Gros, S. Rodriguez-Mozaz, C. Delerue-Matos, A. Pena, D. Barceló, M. C. B. Montenegro, *Sci. Total Environ*. **2013**, *461-462*, 302.
[23] M. Patel, R. Kumar, K. Kishor, T. Mlsna, C. U. Pittman, D. Mohan, *Chem. Rev*. **2019**, *119*(6), 3510.
[24] P. K. Thai, L. X. Ky, V. N. Binh, P. H. Nhung, P. T. Nhan, N. Q. Hieu, N. T. Dang, N. K. B. Tam, N. T. K. Anh, *Sci. Total Environ*. **2018**, *645*, 393.
[25] H. Chen, L. Jing, Y. Teng, J. Wang, *Sci. Total Environ*. **2018**, *618*, 409.
[26] M. C. Danner, A. Robertson, V. Behrends, J. Reiss, *Sci. Total Environ*. **2019**, *664*, 793.
[27] Y. Hu, L. Jiang, T. Zhang, L. Jin, Q. Han, D. Zhang, K. Lin, C. Cui, *J. Hazard. Mater*. **2018**, *360*, 364.
[28] T. S. R. Rüger, M. Franchini, T. Trnka, A. Yakovlev, E. van Lenthe, P. Philipsen, T. van Vuren, B. Klumpers, AMS2022.1. **2022**, http://www.scm.com/
[29] D. Dobrin, M. Magureanu, C. Bradu, N. B. Mandache, P. Ionita, V. I. Parvulescu, *Environ. Sci. Pollut. Res*. **2014**, *21*, 12190.
[30] C. Bradu, M. Magureanu, V. I. Parvulescu, *J. Hazard. Mater*. **2017**, *336*, 52.
[31] M. Magureanu, D. Dobrin, C. Bradu, F. Gherendi, N. B. Mandache, V. I. Parvulescu, *Chemosphere* **2016**, *165*, 507.
[32] F. Bilea, C. Bradu, N. B. Mandache, M. Magureanu, *Chemosphere* **2019**, *236*, 124302.
[33] M. Magureanu, N. B. Mandache, C. Bradu, V. I. Parvulescu, *Plasma Process. Polym*. **2018**, *15*(6), 1700201.
[34] J. Villasenor, P. Reyes, G. Pecchi, *Catal. Today* **2002**, *76*(2–4), 121.
[35] B. R. Locke, P. Lukes, J. L. Brisset, *Plasma Chem. Catal. Gases Liq*. **2012**, 185.
[36] M. N. Abellán, B. Bayarri, J. Giménez, J. Costa, *Appl. Catal. Environ*. **2007**, *74*(3–4), 233.
[37] J. O. Back, T. Obholzer, K. Winkler, S. Jabornig, M. Rupprich, *J. Environ. Chem. Eng*. **2018**, *6*(6), 7377.
[38] D. Lee, J. C. Lee, J. Y. Nam, H. W. Kim, *Chemosphere* **2018**, *209*, 901.
[39] E. S. Massima Mouele, T. Z. Myint Myo, H. H. Kyaw, J. O. Tijani, M. Dinu, A. C. Parau, I. Pana, Y. ElOuardi, J. Al-Sabahi, M. Al-Belushi, E. Sosnin, V. Tarasenko, C. Zhang, T. Shao, T. V. Iordache, S. Teodor, K. Laatikainen, A. Vladescu, M. Al-Abri, A. Sarbu, M. Braic, V. Braic, S. Dobretsov, L. F. Petrik, *J. Hazard. Mater. Adv*. **2022**, *5*, 100051.
[40] K. Shang, R. Morent, N. Wang, Y. Wang, B. Peng, N. Jiang, N. Lu, J. Li, *Chem. Eng. J*. **2022**, *431*, 133916.
[41] Y. Wang, J. Huang, H. Guo, C. Puyang, J. Han, Y. Li, Y. Ruan, *Sep. Purif. Technol*. **2022**, *287*, 120540.
[42] K. T. Wong, S. Y. Yoon, S. B. Jang, N. A. Rahman, C. E. Choong, Y. J. Hong, S. E. Oh, E. H. Choi, M. Jang, *Chemosphere* **2023**, *311*, 137003.
[43] H. Zhang, S. Xiao, Y. Du, S. Song, K. Hu, Y. Huang, H. Wang, Q. Wu, *Sep. Purif. Technol*. **2022**, *298*, 121608.
[44] A. Zhang, Y. Zhou, Y. Li, Y. Liu, X. Li, G. Xue, A. C. Miruka, M. Zheng, Y. Liu, *Water Res*. **2022**, *212*, 118128.
[45] F. Bilea, T. Tian, M. Magureanu, H. Rabat, M. -A. Antoissi, O. Aubry, D. Hong, Plasma Process. Polym. **2023**, e2300020. https://doi.org/10.1002/ppap.202300020
[46] J. Martini, C. A. Orge, J. L. Faria, M. F. R. Pereira, O. S. G. Soares, *J. Environ. Chem. Eng*. **2018**, *6*(4), 4054.
[47] P. J. Bruggeman, M. J. Kushner, B. R. Locke, J. G. E. Gardeniers, W. G. Graham, D. B. Graves, R. C. H. M. Hofman-Caris, D. Maric, J. P. Reid, E. Ceriani, D. F. Rivas, J. E. Foster, S. C. Garrick, Y. Gorbanev, S. Hamaguchi, F. Iza, H. Jablonowski, E. Klimova, J. Kolb, F. Krcma, P. Lukes, Z. Machala, I. Marinov, D. Mariotti, S. M. Thagard, D. Minakata, E. C. Neyts, J. Pawlat, Z. L. Petrovic, R. Pflieger, S. Reuter, D. C. Schram, S. Schröter, M. Shiraiwa, B. Tarabová, P. A. Tsai, J. R. R. Verlet, T. vonWoedtke, K. R. Wilson, K. Yasui, G. Zvereva, *Plasma Sources Sci. Technol*. **2016**, *25*(5), 053002.

How to cite this article: P. Brault, F. Bilea, M. Magureanu, C. Bradu, O. Aubry, H. Rabat, D. Hong, *Plasma. Process. Polym*. **2023**, e2300116. https://doi.org/10.1002/ppap.202300116